

Thermal properties of hot and dense medium in interacting hadron resonance gas model

S. Sahoo^{a,b}, D. K. Mishra^{c,1}, P. K. Sahu^{b,2}

^a*Siksha 'O' Anusandhan Deemed to be University, Bhubaneswar 751030, India*

^b*Institute of Physics, HBNI, Sachivalaya Marg, Bhubaneswar, Odisha 751005, India*

^c*Nuclear Physics Division, Bhabha Atomic Research Center, Mumbai 400085, India*

Abstract

The meson exchange interaction based on relativistic mean-field (RMF) theory has been introduced in the hadron resonance gas (HRG) model, called interacting HRG (iHRG) model. This model can be used to explain the experimental data both at finite temperature (T) with finite chemical potential (μ_B) and finite temperature at vanishing chemical potential. The nuclear matter equation of state also can be explained at zero temperature with finite baryon density (finite chemical potential) due to the presence of attractive and repulsive interactions between the hadrons in the iHRG model. Similarly, the lattice equation of state is well described at $\mu_B = 0$ and finite temperature by the iHRG model. In the present study, we have calculated the thermodynamical quantities as a function of temperature and chemical potential using both HRG and iHRG models. Also, we have presented the isothermal compressibility (k_T), specific heat (C_V), and speed of sound (c_s^2) as a function of μ_B , T , and center of mass energies. The effect of kinematic acceptance on these quantities are also presented as a function of μ and T . Results from this study on k_T are compared with results from other heavy-ion transport models and experimental data up to LHC energies.

Keywords: Hadron resonance Gas, relativistic mean-field, thermodynamic parameters

¹dkmishra@barc.gov.in

²pradip@iopb.res.in

1. Introduction

It is expected in nature that with the increase of temperature or baryon density to certain high values in the well-defined system, the system undergoes a change of its physical properties. This change of physical properties is well known as a change of phase transition. Such a phase transition may occur in the strongly interacting system such as nuclear matter and quantum chromodynamics (QCD) matter [1].

Since last two decades, it is a matter of interest that a strongly interacting matter with increasing temperature and baryon density undergoes a phase transition from hadronic to partonic phase, called quark-gluon plasma (QGP) state [2]. To investigate this finding, there are several well established theoretical calculations and experiments on relativistic and ultra-relativistic heavy-ion collisions at very high energies or some are planned for the near future. There are two extreme limits to have phase transition from hadronic matter to partonic matter. These are at a very small temperature with very high baryon densities (in neutron stars) [3, 4] and at small baryon density with very high temperature (at Relativistic Heavy-Ion Collider (RHIC) and Large Hadron Collider (LHC) energies). Another possibility of such phase transition is at moderate temperature and baryons density (Facility for Antiproton and Ion Research (FAIR) energies). At small or vanishing chemical potential or very low baryon density, the lattice QCD calculations suggest a phase transition from hadronic to partonic degrees of freedom is a smooth crossover [5, 6]. The crossover phase transition might transform to first-order phase transition by passing through a critical end point at finite chemical potential or finite baryon density. Besides the lattice QCD [7] calculations, there are other QCD based models [8, 9] at finite chemical potential or finite baryon density, which are well established to explain the phase transition from hadronic to partonic matter and well explain the experimental data from heavy-ion collision experiments.

On the experimental front, there are several experiments performed at RHIC

and LHC energies to study the evidence of the QCD phase transition either directly or indirectly from the physical observables. Of course, there are indirect signatures of phase transition at the small chemical potential with high temperatures at RHIC and LHC energies. But to observe the evidence of this phase transition at higher chemical potential and moderate temperature, new experiments have been planned at the FAIR [10] and the Nuclotron-based Ion Collider Facility (NICA) [11], which will start taking data in the next couple of years.

The hadron-resonance gas (HRG) model is very successful to describe physical observables from relativistic heavy-ion collisions at AGS to RHIC and LHC energies [12, 13]. The basic concept of the model is that the medium created by heavy-ion collisions start equilibrating with time evolution and continue to interact until it reaches to the freeze-out limit. In this model, the hadrons are treated as non-interacting particles. The HRG model successfully describes the particle ratios at finite chemical potential in both canonical and grand canonical approaches. The HRG model reproduce the results of lattice QCD at zero baryon-chemical potential with finite temperature ($T \sim 170$ MeV). Also, the HRG model at finite temperature and chemical potential is very successful in describing the experimental data at RHIC and LHC energies. However, this model fails to describe the nuclear matter properties at finite chemical potential and vanishing or small temperature, such as the nuclear hadronic equation of state at saturation density but works very well at vanishing chemical potential at finite temperature, such as lattice QCD. The reason for failing the HRG model at around nuclear matter saturation regions, because it does not have repulsive and attractive interaction between the hadrons, which are very important when there is interaction in the medium and helps to get saturation properties at nuclear matter. The HRG model works very well at small μ_B and higher T , because the matter leads to an ideal gas of satisfying the thermodynamics description of the particles up to $T \sim 170$ MeV.

To overcome the shortcomings of the HRG model at finite chemical potential or finite baryon density, we have included the repulsive and attractive interaction between baryons in the HRG model through the relativistic mean-

field (RMF) theory [14, 15]. Recently, an attempt has been made to include interactions between baryons based on the RMF theory in the HRG model [16] and repulsive baryon–baryon interactions in a hadron gas model [17]. The RMF models are very good to explain the properties of infinite nuclear matter, such as the gross structure of neutron stars [18] and properties of finite nuclei [19], as the scalar interaction is for attractive and vector interaction is for repulsive potentials, which are included through the meson exchange interactions with proper parameters. However, these models fail to explain the matter at low density or vanishing chemical potential and at finite high temperatures, such as QCD matter. Hence, in the RMF models the QCD matter properties such as specific heat, susceptibility, thermal compressibility and equation of state at finite temperature are not well described.

In view of the above reasons, we adopt a combination of both RMF and HRG models, which we call as iHRG model. Therefore, it may explain both vanishing chemical potential to finite chemical potential with zero to finite temperature i.e. hadronic nuclear matter to QCD matter. In the present study, we consider RMF chiral sigma model [15, 19, 20, 21, 22], which can describe well the ground state properties of infinite nuclear matter, neutron star gross properties and properties of finite nuclei. Along with this model, we combine the HRG model to explain the lattice QCD and heavy-ion collision data at RHIC and LHC at small/vanishing chemical potential and at finite temperature near hadronic to a partonic phase transition.

The paper is organized as follows. In the following sections II and III, we describe the ideal HRG model and interacting HRG (iHRG) model, with subsections of RMF theory with zero and finite temperature, respectively. The results and discussions are given in section IV and finally, we summarize our findings in section V.

2. Hadron resonance gas model

The HRG model is based on the work of Dashen, Ma, and Bernstein [23], which shows that one can describe the strongly interacting system by a gas of free hadrons and inclusion of resonances in a thermal medium. Further these resonances can be related to phase shift [24, 25]. In this model, the stable hadrons and the resonances are considered as a non-interacting point particles. This simple statistical model is successful in describing the particle abundances in nucleon-nucleus [26], and heavy-ion collisions for different collision energies typical of Alternating Gradient Synchrotron (AGS) up to those of the Large Hadron Collider (LHC) [27, 28, 29]. The HRG model is also successfully applied to smaller systems such as: $p + p$ [30] and $e^+ + e^-$ collisions [31]. It has been observed that, ideal HRG model is quite successful in reproducing the Lattice QCD (LQCD) calculations of the thermodynamic parameters of QCD matter at $\mu \approx 0$ and below temperature $T \approx 170$ MeV. However, the disagreement between LQCD and HRG model calculations are observed at higher temperatures as well as even at low temperature for fluctuations [17, 32].

The heavy-ion experiments cover only a limited phase space, so one can access only a part of the fireball produced in the collision, which resembles the grand canonical ensemble (GCE) [33, 34]. There is no requirement of conservation of energy, momentum, and charge measured in the limited phase-space in the GCE model, which is similar to the experimental situation in heavy-ion collisions. The thermodynamic potential for the hadronic system is given by the sum of the potential of all stable hadrons and all known resonances. Assuming a thermal system produced in the heavy-ion collisions, the logarithm of the partition function of a hadron resonance gas in the grand canonical ensemble can be written as $\ln Z = \sum_i \ln Z_i$, where the sum is over all the stable hadrons and resonances. In the ambit of GCE framework, the logarithm of the partition function of i -th particle is given as

$$\ln Z_i(T, V, \mu_i) = \pm \frac{V g_i}{(2\pi)^3} \int d^3 k \ln [1 \pm \exp\{(\mu_i - E)/T\}], \quad (1)$$

where V is the volume of the thermal system, g_i being the degeneracy factor for i -th particle, T is the temperature and μ_i is the chemical potential. The single-particle energy $E = \sqrt{k^2 + m^2}$, where m is the mass of the particle and k being the momentum. The \pm sign corresponds to the fermion and boson respectively. All the hadrons having mass up to 2.5 GeV as listed in the PDG are considered in the present calculations. Using partition function one can calculate various thermodynamical quantities of the thermal system formed in heavy-ion collisions. The pressure (P), energy density (ε), number density (n) of the thermal system is defined as:

$$P = \sum_i \pm \frac{g_i T}{2\pi^2} \int_0^\infty k^2 dk \ln[1 \pm \exp\{(\mu_i - E_i)/T\}], \quad (2)$$

$$\varepsilon = \sum_i \frac{g_i}{2\pi^2} \int_0^\infty \frac{k^2 dk}{\exp[(E_i - \mu_i)/T] \pm 1} E_i, \quad (3)$$

$$n = \sum_i \frac{g_i}{2\pi^2} \int_0^\infty \frac{k^2 dk}{\exp[(E_i - \mu_i)/T] \pm 1}. \quad (4)$$

Using the above equations, one can calculate the other thermodynamical quantities such as entropy density (s), square of speed of sound (c_s^2), specific heat (C_V), and isothermal compressibility (k_T) as follows. The pressure and energy density produce at the early stages of the collisions which leads to an increase in entropy density. Entropy being directly related to the experimentally measured charged-particle multiplicity in a given pseudorapidity range is an important observable to study the QCD phase transition. In thermodynamics, it is defined as

$$s = \frac{\varepsilon + P - \sum_i \mu_i n_i}{T}. \quad (5)$$

In hydrodynamics, the speed of sound plays an important role in understanding the equation-of-state and hence, the associated phase transition. It is related to the small perturbations produced in the medium formed in heavy-ion collisions. It explains the rate of change of pressure gradients due to the change in the energy density of the created dense medium. It is defined as

$$c_s^2 = \frac{dP}{d\varepsilon}. \quad (6)$$

The heat capacity or the specific heat (C_V) is a thermodynamic quantity characterizing the equation of state of the system. It is also related to the change in entropy of the thermal system with a change in temperature ($ds = \int \frac{C_V}{T} dT$). In the case of a system undergoing a phase transition, C_V is expected to diverge at the critical point. Close to the critical point, the specific heat is expressed in terms of power-law as $C_V \propto |T - T_c|^{-\alpha}$, where T_c is the critical temperature and α being the critical exponent. The specific heat at constant volume is defined as,

$$C_V = \frac{d\varepsilon}{dT}. \quad (7)$$

Isothermal compressibility (k_T) the measure of the relative change in volume with respect to change in pressure at a constant temperature. Similar to C_V , the k_T is also diverge at the critical point and close to the critical point, it can be expressed in terms of power-law. Hence, the determination of C_V and k_T may help in understanding the critical point and the phase transition and their nature. The isothermal compressibility is defined as

$$k_T = -\frac{1}{V} \frac{dV}{dP} = \frac{1}{V} \frac{\sum_i \frac{dn_i}{d\mu_i}}{\sum_i \left(\frac{dP}{d\mu_i}\right)^2}. \quad (8)$$

The above pressure (P) and energy density (ε) may be represented as (P_{HRG}) and (ε_{HRG}), respectively for ideal (non-interacting) hadron resonance gas model.

3. Interacting Model and Interacting HRG model

The nuclear equation of state (EOS) is very important in nuclear physics and astrophysics [35, 36, 37, 38], specially the liquid-gas phase transition at lower density and finite temperature calculation of nuclear many-body system [39, 40]. To study the properties of quark gluon plasma (QGP) at extreme densities and temperatures [41] and the study of stellar evolution, the global properties of neutron star and supernova explosion [18, 42, 43, 44], the nuclear EOS is also needed.

Theoretically, many-body approaches such as Hartee-Fock, Thomas-Fermi and mean-field theory type procedures [45, 46] have been adopted to derive

the EOS. One of the very successful theoretical calculation of finite nuclei and infinite nuclear matter [18, 19, 20, 41] is the relativistic mean-field (RMF) theory. To describe the required values of saturation properties of nuclear matter, incompressibility, binding energy, and effective nucleon mass, the original Walecka RMF model [47] has been extensively modified. The non-linear term in RMF [48] has been introduced to describe the finite nuclei properties and the nuclear matter properties at normal nuclear density, however, it differs from the relativistic Dirac-Brueckner-Hartree-Fock (DBHF) EOS [49]. Therefore, there are several models, which attempt to reproduce the reasonable EOS, compatible with DBHF, by including vector mesons self couplings.

One such model in the high density nuclear matter [15] is the chiral sigma (CS) model. Like RMF model, the CS model is very successful. The meson fields are calculated similar way based on the mean-field approximation. The non-linear terms here behave like the three-body forces and are main ingredients to reproduce the properties of nuclear matter saturation. We had adopted a SU(2) CS model in the beginning, where the mass of the iso-scalar vector field is generated dynamically [15], however, high value of incompressibility was the main shortcoming. To get desired values of compressibility, effective mass, binding energy, and saturation density, the higher-order terms of the scalar meson field [19, 21, 22], were introduced. Using non-linear SU(2) CS model, we evaluate the nuclear EOS at zero and finite temperature. In this calculation, we choose the stable parameter STO-5 from Ref. [19] and evaluate the thermodynamic quantities, which are the applicable to various heavy-ion collision experiments.

3.1. The Formalism of Chiral Sigma Model

The SU(2) chiral sigma Lagrangian can be written as [15]

$$\begin{aligned} \mathcal{L} = & \frac{1}{2}(\partial_\mu \pi \cdot \partial^\mu \pi + \partial_\mu \sigma \partial^\mu \sigma) - \frac{1}{4}F_{\mu\nu}F_{\mu\nu} \\ & - \frac{\lambda}{4}(x^2 - x_o^2)^2 - \frac{\lambda b}{6m^2}(x^2 - x_o^2)^3 - \frac{\lambda c}{8m^4}(x^2 - x_o^2)^4 \end{aligned}$$

$$\begin{aligned}
& - \sum_i g_{i\sigma} \bar{\psi}_i (\sigma + i\gamma_5 \boldsymbol{\tau} \cdot \boldsymbol{\pi}) \psi_i + \bar{\psi}_i (i\gamma_\mu \partial^\mu - g_{i\omega} \gamma_\mu \omega^\mu) \psi_i \\
& + \frac{1}{2} g_{N\omega}^2 x^2 \omega_\mu \omega^\mu + \frac{1}{24} \xi g_{N\omega}^4 (\omega_\mu \omega^\mu)^2
\end{aligned} \tag{9}$$

Here $F_{\mu\nu} \equiv \partial_\mu \omega_\nu - \partial_\nu \omega_\mu$ and $x^2 = \pi^2 + \sigma^2$. In the Lagrangian ψ_i is for nucleons, Δ , Λ , Σ^- and Ξ hyperons (denoted by subscript i), $\boldsymbol{\pi}$ is the pseudoscalar-isovector pion field and σ is the scalar field. We consider in natural units with $\hbar = c = k_B = 1$.

The main point in this Lagrangian is that it has a dynamically generated iso-scalar vector field, ω_μ , with conserved baryonic current $j_\mu = \bar{\psi} \gamma_\mu \psi$. The constant parameters b and c are included in the higher-order self-interaction of the scalar field in the potential to describe the nuclear saturation density. The modified non-linear CS model is defined by STO-5 in our following discussions. In the fourth-order term in the omega fields, the quantity ξ is a constant parameter. For simplicity, we set ξ to zero. A mass is generated when the interactions of the scalar and the pseudoscalar mesons with the vector meson take place through the spontaneous breaking of the chiral symmetry.

The masses of the nucleon, the scalar meson and the vector meson are respectively given by

$$m = g_\sigma x_o, \quad m_\sigma = \sqrt{2\lambda} x_o, \quad m_\omega = g_\omega x_o, \tag{10}$$

where x_o is the vacuum expectation value of the σ field, $\lambda = (m_\sigma^2 - m_\pi^2)/(2f_\pi^2)$, with m_π is the pion mass and f_π the pion decay coupling constant, and $g_{N\omega} = g_\omega$ and $g_{N\sigma} = g_\sigma$ are the coupling constants for the vector and scalar fields, respectively. In the mean field approximation, we assume the pion field to be zero because of it's pseudoscalar in nature. However, there is an interaction between nucleon and pion. The inclusion of pions in the thermodynamic trace is due to $\langle \delta\pi \delta\pi \rangle$ propagator, with an interacting pion mass determined from the RMF model.

By adopting mean-field approximation, the equation of motion of fields is obtained. This approach has been used extensively to evaluate the equation of state in any theoretical models for high density and finite temperature of the

nuclear matter.

The equation of motion for the scalar field is given below based on the ansatz of mean-field

$$(1 - R^2) - \frac{b}{m^2 c_\omega} (1 - R^2)^2 + \frac{c}{m^4 c_\omega^2} (1 - R^2)^3 + \frac{2c_\sigma c_\omega n_B^2}{m^2 R^4} - \sum_i \frac{c_\sigma \gamma}{\pi^2} \int_0^{k_F} \frac{k^2 dk}{\sqrt{k^2 + m_i^{*2}}} = 0, \quad (11)$$

where $m^* \equiv Rm$ is the effective mass of the nucleon. The terms $c_\sigma \equiv g_\sigma^2/m_\sigma^2$ and $c_\omega \equiv g_\omega^2/m_\omega^2$ are scalar and vector coupling constants, respectively.

The equation of motion for the iso-scalar vector field is

$$\omega_0 = \frac{g_\omega x^2 \gamma}{(2\pi)^3} \int_0^{k_F} d^3k. \quad (12)$$

The quantity k_F is the Fermi momentum and the degeneracy factor γ is the nucleon spin.

3.2. Hadronic matter at finite temperature

The equation of state for finite temperature is as follows:

$$\begin{aligned} \varepsilon_{RMF}(T) &= T1 - T2 + T3 + T4 \\ &\quad + \frac{\gamma}{2\pi^2} \sum_i \int_0^\infty k^2 dk \sqrt{k^2 + m_i^{*2}} (d_i(T) + \bar{d}_i(T)), \\ P_{RMF}(T) &= -T1 + T2 - T3 + T4 \\ &\quad + \frac{\gamma}{6\pi^2} \sum_i \int_0^\infty \frac{k^4 dk}{\sqrt{k^2 + m_i^{*2}}} (d_i(T) + \bar{d}_i(T)). \end{aligned} \quad (13)$$

Where,

$$\begin{aligned} T1 &= \frac{m^2(1 - R^2)^2}{8c_\sigma}, \\ T2 &= \frac{b}{12c_\omega c_\sigma} (1 - R^2)^3, \\ T3 &= \frac{c}{16m^2 c_\omega^2 c_\sigma} (1 - R^2)^4, \\ T4 &= \frac{c_\omega n_B^2}{2R^2}. \end{aligned} \quad (14)$$

The baryon and scalar densities at finite temperature are respectively defined as

$$\begin{aligned}
n_B(T) &= \frac{\gamma}{(2\pi)^3} \sum_i \int_0^\infty d^3k (d_i(T) - \bar{d}_i(T)), \\
n_S(T) &= \frac{\gamma}{(2\pi)^3} \sum_i \int_0^\infty \frac{m_i^* d^3k}{\sqrt{k^2 + m_i^{*2}}} (d_i(T) + \bar{d}_i(T)).
\end{aligned} \tag{15}$$

The Eq. 11 is modified as

$$\begin{aligned}
& (1 - R^2) - \frac{b}{m^2 c_\omega} (1 - R^2)^2 \\
& + \frac{c}{m^4 c_\omega^2} (1 - R^2)^3 + \frac{2c_\sigma c_\omega n_B^2}{m^2 R^4} \\
& - \sum_i \frac{c_\sigma \gamma}{\pi^2} \int_0^\infty \frac{k^2 dk}{\sqrt{k^2 + m_i^{*2}}} (d_i(T) + \bar{d}_i(T)) = 0.
\end{aligned} \tag{16}$$

The distributions functions for nucleon $d(T)$ and anti-nucleon $\bar{d}(T)$, are respectively, given as

$$\begin{aligned}
d_i(T) &= \sum_i \frac{1}{\exp[(E_i^* + \mu_i^*)/T] + 1} \\
& \qquad \qquad \qquad \& \\
\bar{d}_i(T) &= \sum_i \frac{1}{\exp[(E_i^* - \mu_i^*)/T] + 1}.
\end{aligned} \tag{17}$$

where $E_i^* = \sqrt{k^2 + m_i^{*2}}$, T is temperature.

Since the Lagrangian above includes nucleons, hyperons, σ , and ω mesons, the meson fields interact with baryons through linear coupling. The coupling constants are different for non-strange and strange baryons. The ω mass is chosen to be physical masses. The equation of state is obtained through the mean field ansatz. In this case, one can define effective masses (m_i^*) and chemical potentials (μ_i^*) for the baryons as

$$\begin{aligned}
m_i^* &= -g_{i\sigma}\sigma_0 \\
\mu_i^* &= \mu_i - g_{i\omega}\omega_0,
\end{aligned} \tag{18}$$

where ω_o , and σ_o are the non-zero vacuum expectation values of the meson fields.

3.3. Hadronic matter at zero temperature

The equation of state is calculated from the diagonal components of the conserved total stress tensor corresponding to the Lagrangian together with the mean-field equation of motion for the fermion field and a mean-field approximation for the meson fields. The total energy density, ε , and pressure, P of the many-nucleon system are defined as the following:

$$\begin{aligned}\varepsilon_{RMF}(0) &= T1 - T2 + T3 + T4 \\ &\quad + \frac{\gamma}{2\pi^2} \sum_i \int_o^{k_F} k^2 dk \sqrt{k^2 + m_i^{*2}}, \\ P_{RMF}(0) &= -T1 + T2 - T3 + T4 \\ &\quad + \frac{\gamma}{6\pi^2} \int_o^{k_F} \frac{k^4 dk}{\sqrt{k^2 + m_i^{*2}}}.\end{aligned}\tag{19}$$

The energy per nucleon is $E/A = \varepsilon/n_B$, where $\gamma = 4$ for symmetric nuclear matter.

The baryon n_B and scalar densities n_S are respectively defined as

$$\begin{aligned}n_B &= \frac{\gamma}{(2\pi)^3} \sum_i \int_o^{k_F} d^3k, \\ n_S &= \frac{\gamma}{(2\pi)^3} \sum_i \int_o^{k_F} \frac{m^*}{\sqrt{k^2 + m_i^{*2}}} d^3k,\end{aligned}\tag{20}$$

these are used in Eq.(11).

3.4. Interacting HRG model

The thermodynamic quantities and equation of states are calculated using both the ideal HRG model as well as interacting HRG (iHRG) model. The energy density and pressure are defined in iHRG model as

$$\begin{aligned}
\varepsilon_{iHRG} &= \varepsilon_{RMF} + \varepsilon_{HRG} - \varepsilon_N - \varepsilon_\Delta \\
P_{iHRG} &= P_{RMF} + P_{HRG} - P_N - P_\Delta
\end{aligned}
\tag{21}$$

Where ε_N , ε_Δ , P_N and P_Δ represent the energy density and pressure of the non-interacting nucleons and deltas in the HRG model. The interaction for all baryons such as nucleons (N) and Deltas (Δ) are taken as same as nucleons. However, for hyperonic baryons, the interaction is taken as described below.

The nonlinear RMF hadronic model has a couple of parameters, which are determined by the properties of nuclear matter. The nucleon couplings to scalar (g_σ/m_σ), and vector mesons (g_ω/m_ω) and the two coefficients b and c in Eq. 11, are obtained by fitting saturation values of nuclear matter binding energy per nucleon (~ -14.5 MeV) and baryon density (~ 0.14 fm $^{-3}$), and Landau mass ($0.85 m_N$). We have taken the stable set of parameters STO-5, given in Ref. [19]. The coupling constant parameters of the hyperon (ratio of hyperon-meson and nucleon-meson) are uncertain because hyperons do not present in the nuclear matter, hence cannot be determined from the nuclear matter properties. Therefore, we choose the value of hyperon couplings for scalar and vector mesons as 2/3 (similar to quark counting value for Λ , Σ and Ξ). The detail is referred to Refs. [3, 4] and references therein.

4. Results and discussion

Figure 1 shows the binding energy as a function of baryon density at zero temperature for both HRG and iHRG models. The parameters are considered in such a way that the iHRG model can describe the required saturation density and binding energy at the ground state of nuclear matter. In the iHRG model, interactions between baryons are based on the relativistic mean-field theory. Further, the repulsive and attractive interactions are introduced through meson-exchange reaction. We have used the same particles in the iHRG model along with all resonance particles as used in the HRG model. The solid red line

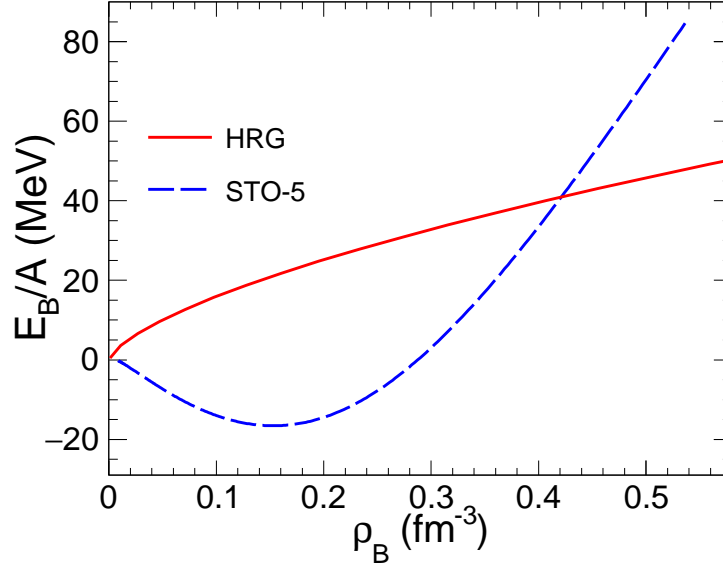


Figure 1: The binding energy per nucleon (E_B/A) as a function of nucleon density (ρ_B) at $T = 0$. The solid red line is the result from the ideal HRG model and the dashed blue line is for interacting HRG model.

represents the binding energy per nucleon for non-interacting nucleons with all resonances in the HRG model. The dashed blue line shows the equation of state of iHRG used in the HRG model. Since there is no interaction among the nucleons in the HRG model, so the binding energy at saturation density does not reproduce the ground state value of normal nuclear matter. Figure. 2 shows the ratios of effective masses to the bare masses as a function of temperature at different μ (Fig. 2a) and as a function of baryon chemical potential at different T (Fig. 2b). The dotted lines shown in both the figures correspond to the calculations from the non-interacting (ideal) HRG model in which the mass of the hadrons are same as their rest mass (m_0). In Fig 2a, the effective mass remains at their vacuum values up to $T \approx 150$ MeV at lower baryon chemical potential (up to $\mu \sim 200$ MeV). In case of higher $\mu \sim 500$ MeV, the effective mass starts reducing even at lower $T \sim 70$ – 80 MeV. In Fig 2b, the effective mass remains unchanged as the vacuum values up to $\mu \sim 400$ MeV for $T = 100$ MeV

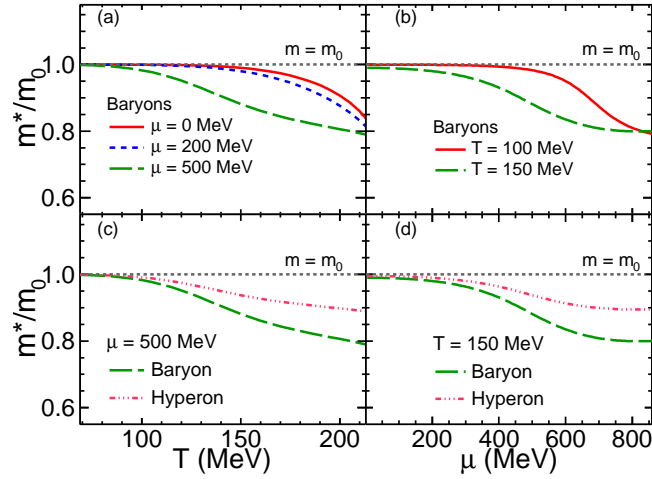


Figure 2: Ratios of the effective mass (m^*) of the baryons (hyperons) relative to their rest mass (m_0) as a function of T for difference μ values (panel (a)) and function of μ for different T values (panel (b)). The ratios of effective masses of hyperons as a function of T (panel (c)) and function of μ (panel (d)).

and there is sudden decrease of effective mass with increase in μ . For higher temperature ($T \geq 150$ MeV) there is 2–3% reduction of effective mass upto $\mu = 200$ MeV, thereafter gradual decrease as a function of μ . The choices of T up to 150 MeV and $\mu = 500$ MeV are taken, because these higher values of T and μ can be reached in heavy-ion collision experiments. In the lower two panels Fig. 2c and Fig. 2d shows the reduced mass ratios for baryons and hyperons as a function of T and μ , respectively. The effective mass of baryons reduces significantly with increasing temperature and baryon density. This reduction is due to increase in attractive force between baryons in the nuclear matter as a function of temperature and baryon density. However, in the ideal HRG model, the masses of baryons remain constant due to the absence of interaction between the hadrons. Recently in the hadron resonance gas model [50], it has been investigated the fluctuations and correlations involving baryon number in hot hadronic matter considering the in-medium mass effect of baryons. The effective mass is used in the rest of the present study.

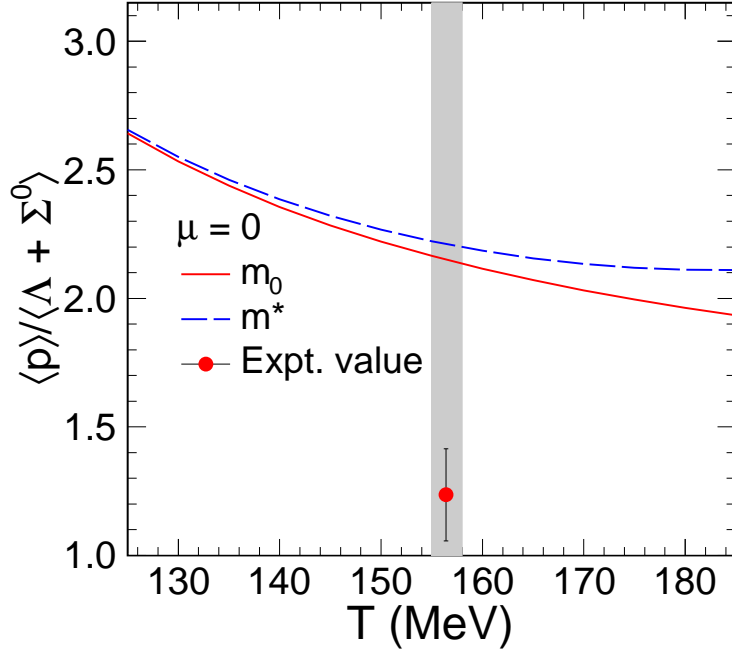


Figure 3: The ratio of proton to that of $\Lambda + \Sigma^0$ baryons as a function of T . The solid red line is the result from the ideal HRG model and the dashed blue line is for interacting HRG model. The solid symbol depicts the experimental value measured by the ALICE collaboration for the most central Pb-Pb collisions (at $\sqrt{s_{NN}} = 2.76$ TeV) [51, 52, 53].

As discussed in the previous section about the value of hyperon couplings for scalar and vector mesons, we have constructed a volume independent quantity, the ratios of the yields of protons to that of $\Lambda + \Sigma^0$ baryons. Figure 3 shows the ratios as a function of T for both ideal and interacting HRG models. The ratio provides an useful diagnostic for the particle content, hence the interaction strengths, in the baryon sector. The interacting model shows an increase in the ratios relative to the ideal HRG case. Within the HRG model, at around $T = 150$ – 160 MeV, the ratio is slightly above 2.0, and the interacting HRG model leads to further increase in the ratio. However, the experimental data obtained by ALICE collaboration on (multi)strange particle production in Pb+Pb collisions at $\sqrt{s_{NN}} = 2.76$ TeV [51, 52, 53] suggests that the value is around 1.3,

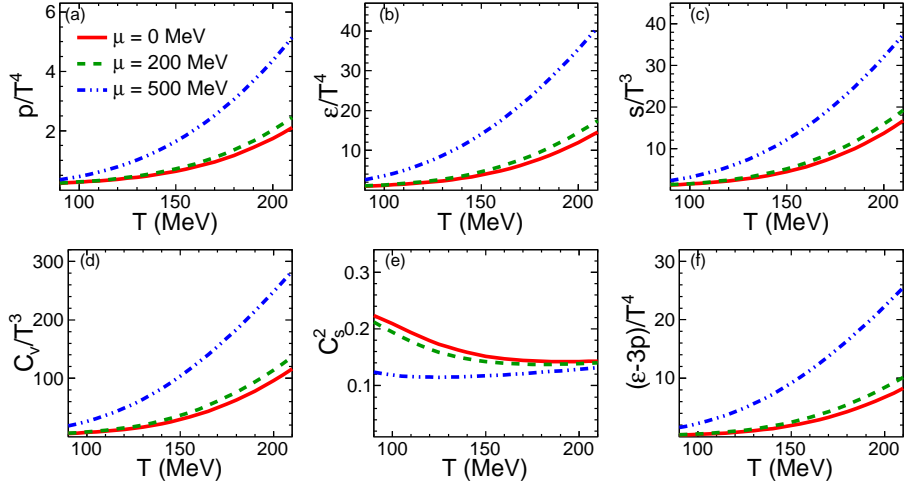


Figure 4: The variation of different thermodynamic quantities (p/T^4 , ϵ/T^4 , s/T^3 , C_V/T^3 , c_s^2 , and $(\epsilon - 3p)/T^4$) as a function of T for $\mu = 0$ (solid red line), 200 MeV (dashed green line), and 500 MeV (dotted-dashed blue line) calculated using ideal HRG model.

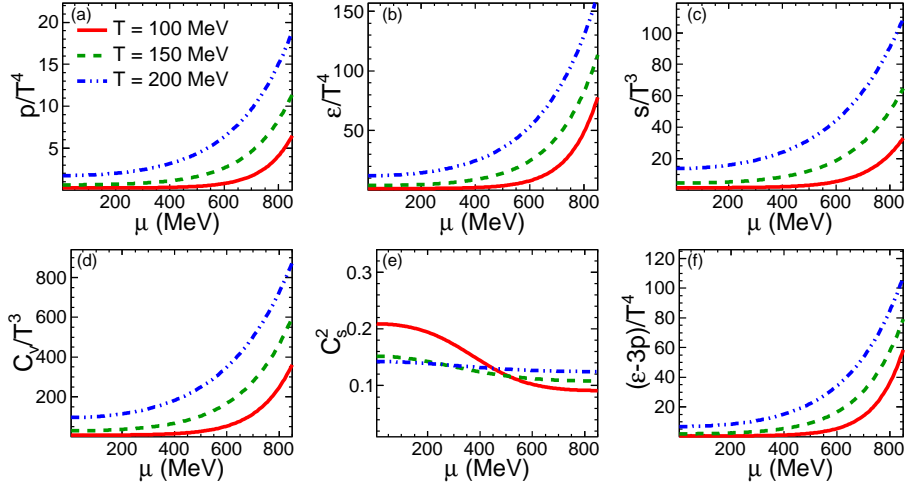


Figure 5: The variation of different thermodynamic quantities as shown in Fig. 4 as a function of μ for different values of $T = 100$ MeV (solid red line), 150 MeV (dashed green line) and 200 MeV (dotted-dashed blue line) using ideal HRG model.

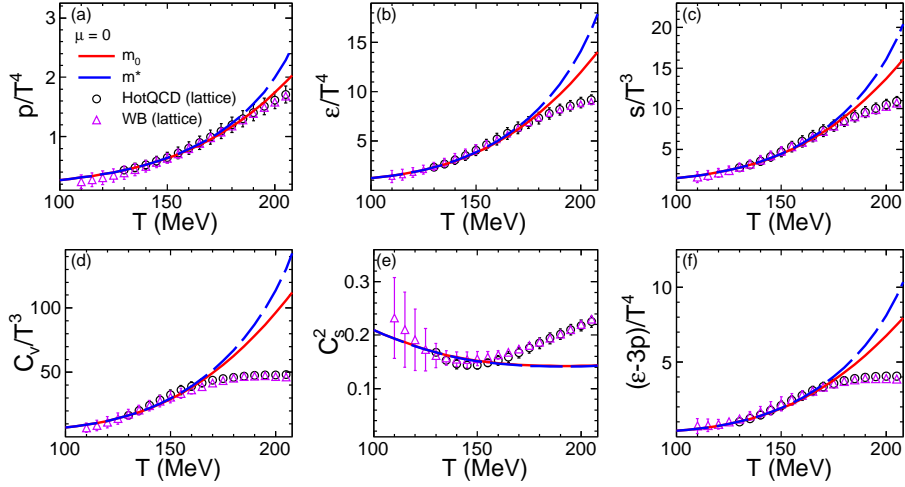


Figure 6: The equation of states of interacting HRG (iHRG) as a function of temperature T . The solid red line for ideal HRG model (with $m = m_0$) and blue dashed line for iHRG (with $m = m^*$) model. The open circle and magenta triangle symbols are for HotQCD [56] and WB [57] lattice data respectively.

which is significantly lower than the HRG result, and also goes against the trend demonstrated by the iHRG model. The value of 1.3 in the experimental data may be explained by: a suppressed proton yield [54] with non-resonant interaction and an increase in hyperon yield. Further, the non-resonant interaction can include dynamical features like roots, and coupled-channel effects [55]. These effects are absent in the present RMF base iHRG model, and could be a reason why results from iHRG model displayed the opposite trend to data.

Figure 4 shows the thermodynamic parameters (p/T^4 , ε/T^4 , s/T^3 , C_V/T^3 , c_s^2 , and $(\varepsilon - 3p)/T^4$) as a function of temperature for different $\mu = 0, 200$ MeV, and 500 MeV. These parameters are calculated with ideal case of the HRG model. It is observed that the values of thermodynamic parameters as a function of T are the same for any value of μ up to 200 MeV. However, there is a significant difference at higher baryon chemical potential. This indicates, when the baryon density increases along with temperature, the system is more excited and the production of particles are more as a result, the pressure and

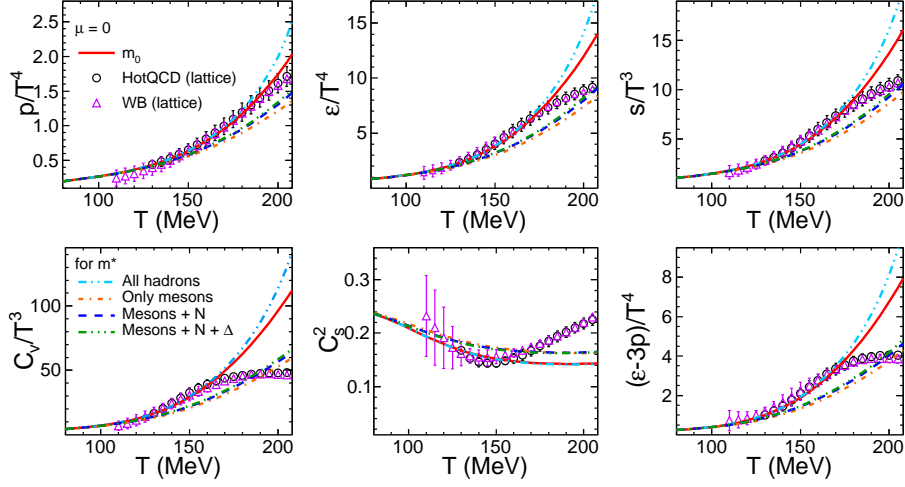


Figure 7: The equation of states of interacting HRG (iHRG) as a function of temperature T . There are five choices of equation of states: for all particles with $m = m_0$ (solid red line), for all hadrons with $m = m^*$ (dashed double dots cyan line), for only mesons (dashed dotted orange line), mesons with only nucleons (blue dashed line), mesons along with nucleons and deltas resonances (green dashed triple dot line). The open circle and magenta triangle symbols are for HotQCD [56] and WB [57] lattice data respectively.

energy density increase as a function of temperature. However, the square of speed of sound decreases as a function of temperature, which implies that the rate of change of energy density is faster than the pressure due to more excited thermal energy and more number of degrees of freedom. At higher temperature, the square of speed of sound for all three chemical potential tends to similar values. That may be the region where the nuclear matter changes its phase structure.

Figure 5 shows the thermodynamical parameters (p/T^4 , ϵ/T^4 , s/T^3 , C_V/T^3 , C_s^2 , and $(\epsilon - 3p)/T^4$) as a function of chemical potential for different $T = 100$ MeV, 150 MeV and 200 MeV. These parameters are calculated with ideal case of HRG mode same as shown in Fig. 4. It is observed that for different values T (100 MeV, 150 MeV and 200 MeV), there is a systematically increase in the values of thermodynamic parameters as a function of μ for different

temperatures. However, in case of the square of speed of sound for $T = 100$ MeV and 150 MeV, the change is very insignificant as a function of chemical potential or high baryon density. It clearly says that at around $T \sim 150$ MeV and above, the system is in another state of matter, may be a phase transition to exotic matter, the proportionate change of pressure with respect to energy density is the same as a function of chemical potential.

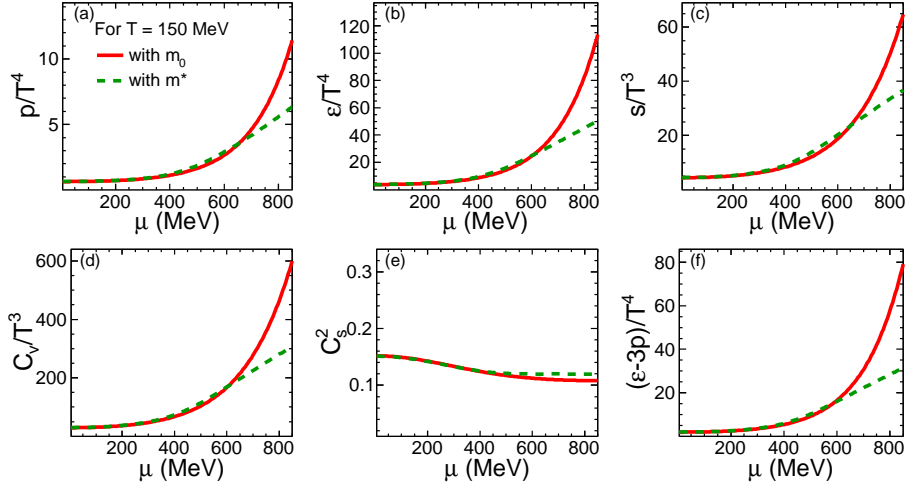


Figure 8: The equation of states of interacting HRG (iHRG) as a function of μ at $T = 150$ MeV. The solid red line is for HRG calculations using $m = m_0$ and the dashed green line is for iHRG calculations using $m = m^*$.

The thermodynamical parameters (p/T^4 , ϵ/T^4 , s/T^3 , C_V/T^3 , c_s^2 , and $(\epsilon - 3p)/T^4$) as a function of temperature at zero chemical potential calculated using HRG and iHRG models are shown in Fig. 6. The HRG and iHRG results are compared with the lattice QCD results of the Hot-QCD Collaboration [56] and the Wuppertal-Budapest (WB) Collaboration [57] shown in the same figure. The solid red line is for the HRG model and the blue dashed line is for iHRG model. The lattice data are very well described by both the models up to $T \sim 180$ MeV. In case of C_V/T^3 and c_s^2 data in both models explain up to $T \leq 170$ MeV temperature range. It is very interesting to note that the iHRG model starts showing the difference from the HRG model calculations at temperature

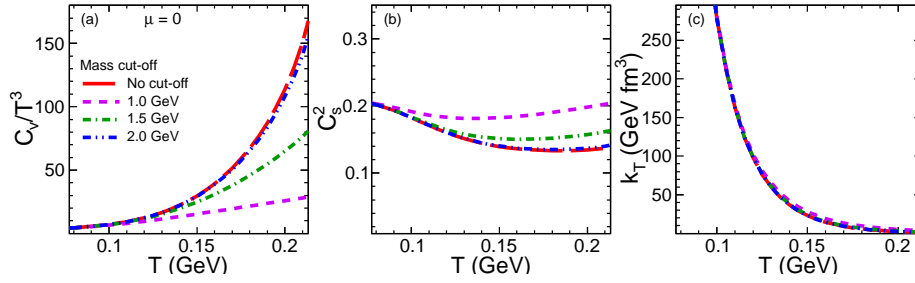


Figure 9: The specific heat C_V/T^3 (panel (a)), speed of sound c_s^2 (panel (b)), and the isothermal compressibility k_T (panel (c)) as a function of T for inclusion of particles of different mass cut-offs at $\mu = 0$ using iHRG model.

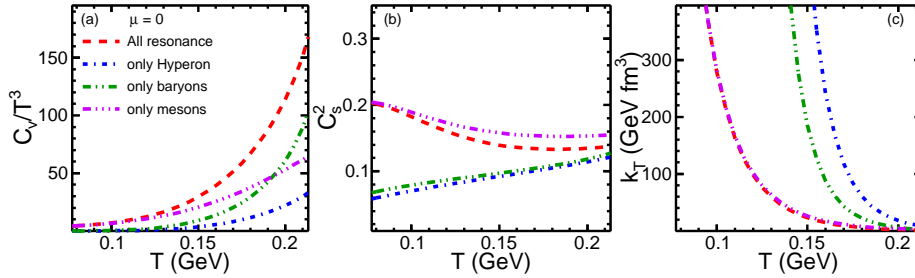


Figure 10: Variation of C_V/T^3 (panel (a)), c_s^2 (panel (b)), and the k_T (panel (c)) as a function of T by taking different type of particles: all resonances (dashed red line), only hayperons (dashed-dotted blue line), only baryons (dashed-double dotted green line), and only mesons (dashed-triple dotted magenta line) at $\mu = 0$ using iHRG model.

above 170 MeV in all thermodynamical parameters. However, in the case of c_s^2 , both the models show almost no difference as a function of temperature. The equation of state, specifically the pressure at a higher temperature and at around the QGP region is more, as a result, the flow of particles from the collisions is more. It is noticed that to explain lattice data, the pressure has to be more harder or more repulsive force due to vector mesons is required at around temperature above 170 MeV.

Fig. 7, shows the same thermodynamical parameters as a function of temperature for different hadron species, where there are all particles using ideal HRG

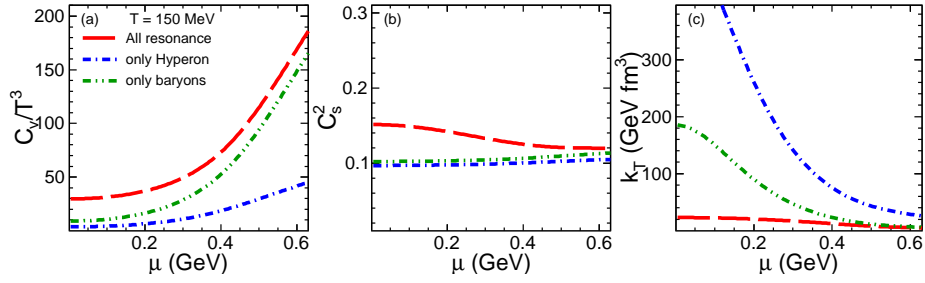


Figure 11: Variation of C_V/T^3 (panel (a)), c_s^2 (panel (b)), and the k_T (panel (c)) as a function of μ by taking different type of particles: all resonances (dashed red line), only hyperons (dashed-dotted blue line), and only baryons (dashed-double dotted green line) at $T = 150$ MeV using iHRG model.

(solid red line), all hadrons (dashed-dotted cyan line), only mesons (dashed orange line), mesons plus nucleons (dashed blue line) and mesons plus nucleons and deltas (dashed-dotted green line) at zero chemical potential in iHRG models. The results from these models are compared with lattice calculations. The lattice data can be well described by both models up to $T \sim 160$ MeV. However, for models with mesons plus nucleons and mesons plus nucleons and deltas are well-matched with data up to temperature 200 MeV within the error bar, except for the square of the sound speed. This indicates that, the temperature above 160 MeV, which is close to the transition temperature to QGP phase, the production of particles are mainly mesons, nucleons and deltas due to Boltzmann suppression in masses. Since the net baryon number (baryons minus anti-baryons) at around high temperature ($T \geq 150$ MeV) and very high center of mass of collision energies, is less, therefore, other heavy baryons may be less around those regions. Another interesting point is noticed in lattice data that at around and above temperature 160 MeV, the speed of sound square shows an increasing trend. However, a slowly decreasing trend is seen in the cases of meson with nucleon and mesons with nucleon and delta baryons, that indicates that the interaction between the particles is soft as compare to lattice results.

In Fig. 8, we compare the thermodynamical parameters as a function of chemical potential at fixed temperature of 150 MeV in both HRG and iHRG models. The thermodynamic parameters from both the models are in good agreement for μ up to 650 MeV, thereafter, there is a significant difference from iHRG to HRG due to strong attractive force, that reflects in the reduction in the mass of the baryons.

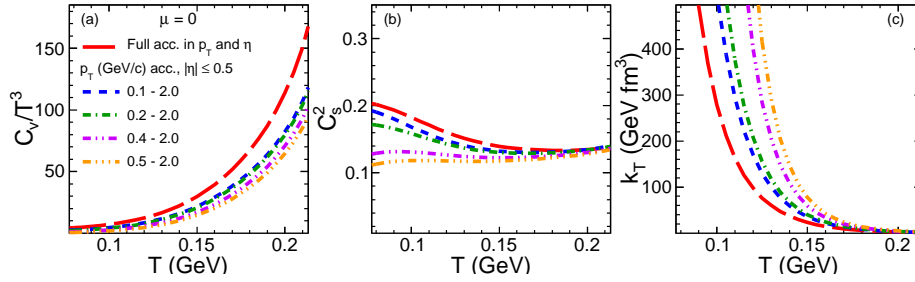


Figure 12: The C_V/T^3 (panel (a)), c_s^2 (panel (b)), and k_T (panel (c)) as a function of T for different p_T acceptances within $|\eta| \leq 0.5$ at $\mu = 0$ using iHRG model. Calculation for full p_T and η acceptance are shown (long dashed red line) for comparison.

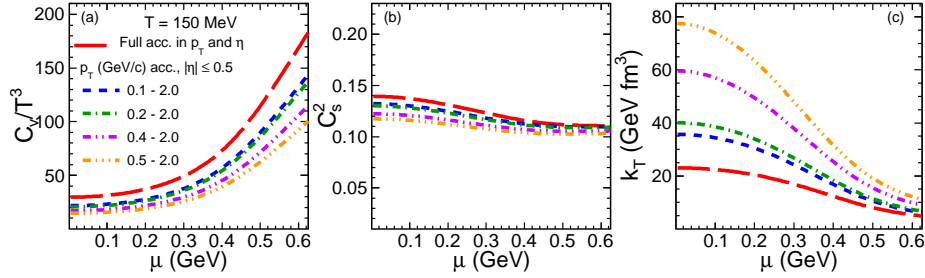


Figure 13: Thermodynamic quantities same as in Fig. 12 as a function of baryon chemical potential μ for different p_T acceptances within $|\eta| \leq 0.5$ at $T = 150$ MeV using iHRG model. Calculation for full p_T and η acceptance are shown (long dashed red line) for comparison.

Figure. 9 shows the C_V/T^3 , c_s^2 , and k_T values are shown as a function of temperature for different higher mass cut-off at $\mu = 0$ in the iHRG model. When higher mass particles are included ($m_0 \geq 1.0$ GeV cut-offs), that means,

increasing the degrees of freedom in the system, thus the ε increases, as a result the C_V (Fig. 9a) increases as a function of temperature, but in case of c_s^2 (Fig. 9b), with increase of mass cut-off then it decreases. At lower T , C_V is dominated by contributions from mesons and at higher T contributions to C_V dominated by heavy baryons. It is clear from this observation that, the change of pressure due to the increase in temperature and increase of degrees of freedom, does not quantify significantly. This can also be verified from k_T plot in (Fig. 9c) as a function of temperature, where k_T does not change to each other with increasing mass cut-off values in the interacting HRG model. However, in the case of the ideal HRG case, it is observed that k_T has a lower value when higher mass resonances added into the system [58]. The k_T values decrease with temperature indicates that the matter formed is denser, hence it is difficult to compress the system. The temperature around phase transition from hadronic to partonic phase, the values of k_T vanish with density, due to the super fluid nature of the quark gluon matter.

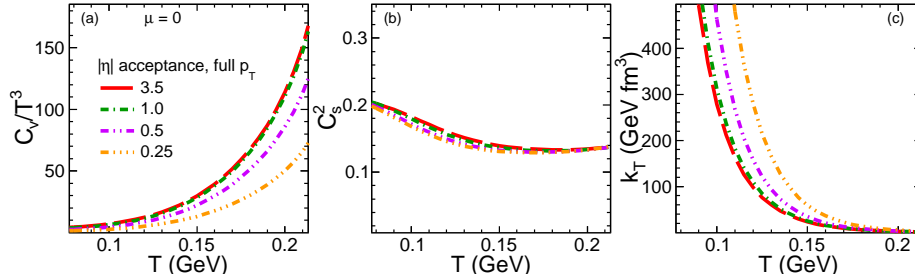


Figure 14: The C_V/T^3 (panel (a)), c_s^2 (panel (b)), and k_T (panel (c)) as a function of T for different η acceptances with full p_T acceptance at $\mu = 0$ using iHRG model.

In Fig. 10, C_V/T^3 , c_s^2 , and k_T values are plotted as a function of temperature at zero chemical potential for different species of the particles in the iHRG model. With the increasing number of degrees of freedom, the total energy density increases as a function of temperature, which can be very much evident in the Fig. 10a. At $T \sim 190$ MeV, the green dashed line with only baryons takes over the magenta dashed line for only mesons, it means that the baryons

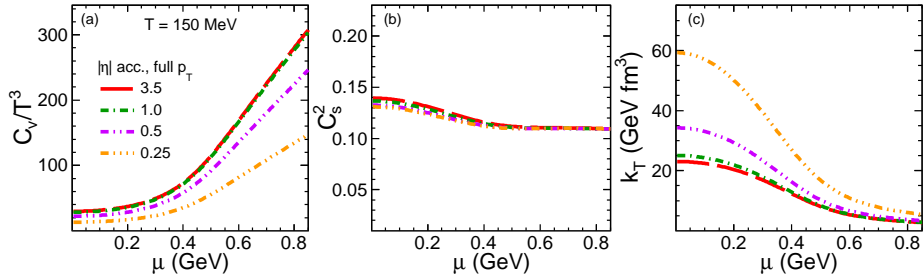


Figure 15: Thermodynamic quantities same as in Fig. 14 as a function of baryon chemical potential μ for different η acceptances with full p_T acceptance $T = 150$ MeV using iHRG model.

energy density is much more than the mesons due to their heavy mass at such high temperatures. In the case of Fig. 10b, the baryon and hyperon lines are much less than all resonances (red dashed line) and all mesons (magenta line). Since the baryons are heavier than mesons and the effect of baryons are much less in medium compare to mesons, therefore, the square of velocity of sound is much less at a lower temperature, however, all resonances, mesons and strange and non-strange baryons tend to vary similar square of velocity of sound at high temperature (≥ 200 MeV). If one observes k_T value with different species, it is clear that the k_T is very small for all the cases at $T \geq 200$ MeV. The baryons start appearing first and then hyperons in the hadronic matter, therefore, the value of k_T for baryons appear first than hyperons at high temperature, as is shown in Fig. 10c. However, the k_T value starts appearing at early value of temperature and reaches close to zero for baryons than the hyperons. After the temperature more than 200 MeV, the k_T vanishes, which means the matter is in the QGP state, which is in a perfect fluid state. A similar trend is also seen in Fig. 11. Here C_V/T^3 , c_s^2 , and k_T values are plotted as a function of chemical potential at fixed temperature 150 MeV in iHRG model. Since there is very less number of hyperons at $T = 150$ MeV and at low chemical potential or low baryon density, the value of C_V/T^3 is less and increases with chemical potential. The C_V/T^3 value is high for all resonances at low chemical due to

the large number of degrees of freedom for all particles. The intermediate value for C_V/T^3 is due to only baryons as seen in the figure includes hyperons and non-strange baryons. Similarly, the speed of sound for all resonance is higher than the only baryons and only hyperons as seen in Fig. (11b). The c_s^2 value is very less dependent on μ at $T = 150$ MeV for only hyperons and only for baryons. In the case of all resonances, the velocity of sound square is high at low density and merges to values of only baryons at high density with fixed quark-gluon plasma temperature $T = 150$ MeV. In Fig. 11c, the k_T value is much less for all resonances as compared to considering only baryons or only hyperons as a function of chemical potential for fixed temperature 150 MeV. We notice here that the mass of baryons and hyperons is higher than resonance particles, therefore, the k_T value is high and slowly goes to zero at high chemical potential and hence high baryon density. So it is hard to compress thermally the matter at low density for hyperons and baryons than high density at a fixed temperature around the quark-gluon transition temperature region.

There are limitations in the experimental measurements, which are a fraction of the total available phase-space. Also, a different experiment may have different kinematic acceptance [59]. Hence, it is important to study the C_V/T^3 , c_s^2 , and k_T as a function of p_T and η acceptance. Figures 12–15 show the C_V/T^3 , c_s^2 , and k_T as a function of chemical potential at fixed T and as a function of temperature at $\mu = 0$ for different p_T and η acceptance range so that the model calculations can be compared with experimental heavy-ion collision data at RHIC and LHC energies. Figures. 12, 13 show the T and μ dependence above three thermodynamic quantities, respectively using iHRG model. The values for full acceptance in p_T and η are shown in the red dashed lines and other p_T acceptance cuts are also shown with $|\eta| < 0.5$. It is observed that there is clear p_T acceptance dependence for C_V/T^3 and k_T as a function of both μ and T . While applying higher momentum cuts, the C_V and k_T show the opposite trend as compared to lower momentum cuts. In the case of c_s^2 , the acceptance effect is observed at lower μ and T values. Also, we noticed that with increasing chemical potential or baryon density, the k_T value decreases and merges each

other for fixed temperature, where the QGP transition is expected.

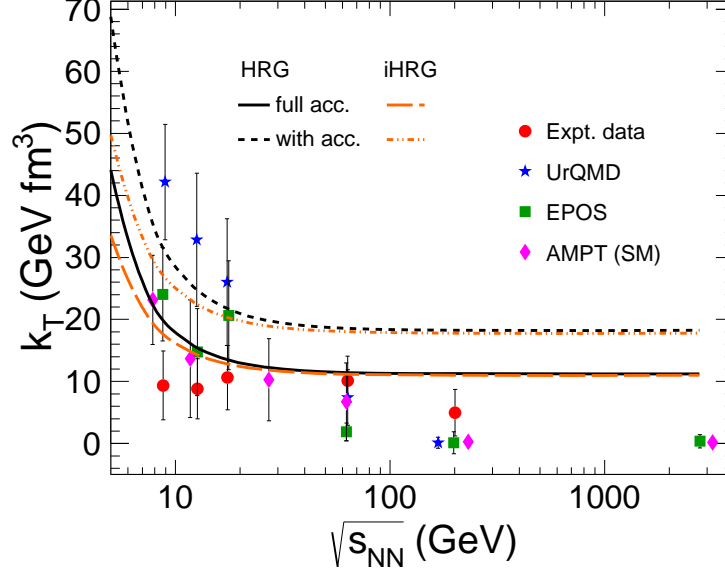


Figure 16: The collision energy dependence of isothermal compressibility k_T calculated using ideal HRG and iHRG models. The model calculations for both full acceptance and limited acceptances are also shown. The transport model calculations from UrQMD, AMPT, and EPOS along with other experimental measurements are shown for comparison (data are taken from [60] and references therein.).

Similar plots of the C_V/T^3 , c_s^2 , and k_T as a function of chemical potential at fixed $T = 150$ MeV and as a function of temperature for $\mu = 0$ with full p_T acceptance range and different η acceptance ranges are shown in Fig. 14 and Fig. 15. The nature of curve in Fig.14(a, c) and Fig. 15(a, c) are very similar to in Fig.12(a, c) and Fig. 13(a, c). However, the c_s^2 values in both the figure Fig.14b and Fig. 15b do not change much and there is no η dependence observed for c_s^2 . This we may interpret as, at temperature close to QGP transition, the matter is having less interaction at lower density.

In order to compare with the experimental measurements, the parameterization of freeze-out parameters μ and T as a function of the center of mass-energy ($\sqrt{s_{NN}}$) are used as given in Ref. [28]. Figure 16 shows the isothermal compress-

ibility as a function of center of mass energies calculated using both for HRG and iHRG models along with results from other heavy-ion transport models and experimental data. The experimental data, red dots are from lower energy to high energy. The other models, UrQMD, EPOS, and AMPT (SM) are denoted as blue star, green square, and magenta diamond symbols, respectively. These model results are taken from [60] and references therein. The HRG and iHRG model calculations are shown for full p_T and η acceptance and $0.2 \leq p_T \leq 2.0$ GeV/ c and $|\eta| \leq 0.5$ acceptances. The effect of acceptance is clearly observed for k_T as a function of $\sqrt{s_{NN}}$. We have noticed that calculations of both HRG and iHRG models for full p_T and η acceptance are close to the data from experiments as well as from other models. However, with selected p_T and η cut-off, the calculated values in both the models are close to other models up to center of mass-energies 20 GeV but overestimate the experimental data for all energies. At low energies up to 10 GeV, the calculations from iHRG model is close to data than HRG model, that is because of the inclusion of interaction between baryons, which is significant at low energies. At high energies, the iHRG and HRG model are very close to each other, there is hardly any difference after 40 GeV of center of mass-energies. From these calculations, it is observed that, isothermal compressibility decreases rapidly with increasing $\sqrt{s_{NN}}$ up to SPS energies (~ 10 to 20 GeV) and remains constant thereafter up to LHC energy. This change of behavior of k_T from lower energy to higher energy could be the onset of phase transition from hadron gas to partonic matter.

5. Summary

In summary, we have studied the thermodynamical quantities at finite temperature with vanishing μ and at finite chemical potential with $T = 0$ using ideal HRG and interacting HRG (iHRG) models. The interaction is introduced through RMF in the HRG model. The interaction terms are based on the MFT among the baryons through meson exchange potential. The attractive interaction is realized by introducing the scalar meson exchange and the repulsive

interaction among the baryons are introduced through vector meson exchange. The iHRG model is able to reproduce the lattice QCD equation of state at $\mu = 0$ with finite temperature and at zero temperature with finite chemical potential or finite baryon density. At finite baryon density with zero temperature, the properties of nuclear matter at saturation density is well explained with a particular set of parameters as well.

In the MFT model, we have taken stable parameters to merge with the HRG model, called as STO-5, which describes well to infinite nuclear matter and data of finite nuclei. There is a substantial effect of interaction on the thermodynamical quantities at higher μ and T values in the iHRG model. Also, the hyperon baryons are taken with proper interaction based on the MFT model. We have taken different options in the iHRG model taking all particles, only baryons, only hyperon baryons, and only resonances.

We have constructed a volume independent quantity, the ratios of the yields of protons to that of $\Lambda + \Sigma^0$ baryons which provides an useful diagnostic for the particle content, hence the interaction strengths, in the baryon sector. Within the HRG model around $T = 150\text{--}160$ MeV, the ratio is slightly above 2.0, and the interacting HRG model leads to further increase in the ratio. However, the experimental result, which is around 1.3 significantly lower than the HRG result, and also goes against the trend demonstrated by the iHRG model. Further, the non-resonant interaction can include dynamical features like roots, and coupled-channel effects. These effects are absent in the present RMF base iHRG model, and could be a reason why results from iHRG model displayed the opposite trend to data. This could be a good motivation for future work on re-examining many of the model assumptions in the RMF model, in comparison to the approach using empirical phase shift.

We have calculated the specific heat, thermal compressibility as well as square of speed of sound using iHRG model as a function of μ and T . The effect of mass cut-off, effects of including hyperons, baryons, and mesons are also presented which show a large effect on the studied quantities. The effect of kinematic acceptances (p_T and η) are studied to compare with the experimental

measurements both as a function of μ and T . The C_V and k_T values are affected by the kinematic consider the acceptance effect while comparing the theoretical models with experimental measurements. The isothermal conductivity is studied as a function of collision energies, which decreases rapidly with increase in $\sqrt{s_{NN}}$ up to SPS energy and remains constant thereafter up to LHC energy. This study provides reference baseline for comparison with the experimental data using purely thermal model and with the inclusion of interaction.

References

- [1] M. A. Stephanov, Prog. Theor. Phys. Suppl. **153**, 139-156 (2004).
- [2] Y. Aoki, Z. Fodor, S. D. Katz and K. K. Szabo, Phys. Lett. B **643**, 46 (2006).
- [3] P. K. Sahu and A. Ohnishi, Nucl. Phys. **A691**, 439-442 (2001).
- [4] G. F. Burgio, M. Baldo, P.K. Sahu and H.-J. Schulz, Phys. Rev. **C66**, 025802-1-14 (2002).
- [5] S. Borsanyi *et al.*, J. High Energy Phys, 08 (2012)126
- [6] H. T. Ding, F. Karsch and S. Mukherjee, Int. J. Mod. Phys, E **24** 1530007 (2015).
- [7] P. Senger *et al.*, Lect. Notes Phys. **814** , 681 (2011).
- [8] V. Vovchenko, M. I. Gorenstein, C. Greiner, and H. Stoecker, Phys. Rev. **C 99**, 045204 (2019).
- [9] P. Costa, C. A. de Sousa, M. C. Ruivo and H. Hansen, Europhys. Lett. **86**, 31001 (2009)
- [10] T. Ablyazimov *et al.* [CBM Collaboration], Eur. Phys. J. A **53**, 60 (2017).
- [11] V. Kekelidze, A. Kovalenko, R. Lednicky, V. Matveev, I. Meshkov, A. Sorin and G. Trubnikov, Nucl. Phys. A **956**, 846 (2016).

- [12] V. Vovchenko, D. V. Anchishkin and M. I. Gorenstein, Phys. Rev. C **91**, 024905 (2015).
- [13] S. Samanta and B. Mohanty, Phys. Rev. C **97**, 015201 (2018).
- [14] B. Datta, and P. K. Sahu, Phys. Lett. **B318**, 277 (1993).
- [15] P. K. Sahu, R. Basu, and B. Datta, Bhaskar, Astrophys. Jour. **416**, 267 (1993).
- [16] T. Steinert and W. Cassing, Phys. Rev. C **98**, 014908 (2018).
- [17] P. Huovinen and P. Petreczky, Phys. Lett. B **777**, 125, (2018).
- [18] P. K. Sahu, Phys. Rev. C **62**, 045801 (2000).
- [19] P. K. Sahu, K. Tsubakihara and A. Ohnishi, Phys. Rev. C **81**, 014002 (2010).
- [20] P. Papazoglou, D. Zschesche, S. Schramm, J. Schaffner-Bielich, H. Stoecker and W. Greiner, Phys. Rev. C **59**, 411 (1999).
- [21] P. K. Sahu, A. Ohnishi, Prog. Theor. Phys. **104**, 1163 (2000).
- [22] P. K. Sahu, T. K. Jha, K. C. Panda, and S. K. Patra, Nucl. Phys. **A733**, 169 (2004).
- [23] R. Dashen, S. K. Ma and H. J. Bernstein, Phys. Rev. **187**, 345-370 (1969).
- [24] P. M. Lo, Eur. Phys. J. C **77**, 533, (2017).
- [25] J. Cleymans, P. M. Lo, K. Redlich and N. Sharma, Phys. Rev. C **103**, 014904, (2021).
- [26] N. Sharma, J. Cleymans and L. Kumar, Eur. Phys. J. C **78**, no.4, 288 (2018).
- [27] P. Braun-Munzinger, K. Redlich and J. Stachel, In *Hwa, R.C. (ed.) et al.: Quark Gluon Plasma 3, 491–599 (2004).

- [28] J. Cleymans, H. Oeschler, K. Redlich and S. Wheaton, Phys. Rev. C **73**, 034905 (2006).
- [29] A. Andronic, P. Braun-Munzinger, K. Redlich and J. Stachel, J. Phys. G **38**, 124081 (2011).
- [30] V. Vovchenko, V. Begun and M. Gorenstein, Phys. Rev. C **93**, 064906 (2016).
- [31] F. Becattini, P. Castorina, A. Milov and H. Satz, Eur. Phys. J. C **66**, 377-386 (2010).
- [32] P. M. Lo, B. Friman, K. Redlich and C. Sasaki, Phys. Lett. B **778**, 454, (2018).
- [33] V. Koch, Chapter of the book "Relativistic Heavy Ion Physics", R. Stock (Ed.), Springer, Heidelberg, 2010, p. 626-652. (Landolt-Boernstein New Series I, v. 23).
- [34] F. Karsch and K. Redlich, Phys. Lett. B **695**, 136 (2011).
- [35] C. Das, R. Sahu and R. K. Tripathi, Phys. Rev. C **48**, 1056 (1993).
- [36] G. Fai and P. Danielwicz, Phys. Lett. B **375**, 5 (1996).
- [37] Y. J. Zhang, R. K. Su, H. Song and F. M. Lin, Phys. Rev. C **54**, 1137 (1996).
- [38] J. Steinheimer, S. Schramm and H. Stoecker, J. Phys. G **38**, 035001 (2011).
- [39] S. Das Gupta, A. Z. Mekjian and M. B. Tsang, nucl-th/0009033
- [40] A. Das, R. Nayak and L. Satpathy, Jour. Phys. G **18**, 869 (1992).
- [41] G.F. Burgio, M. Baldo, P.K. Sahu and H.J. Schulze, Phys. Rev.C **66**, 025802 (2002).
- [42] H. Shen, H. Toki, K. Oyamatsu and K. Sumiyoshi, Nucl. Phys. A **637**, 435 (1998).

- [43] G. Brown, H. Bethe and G. Bayam, Nucl. Phys. A **375**, 481 (1982).
- [44] A. Motornenko, J. Steinheimer, V. Vovchenko, S. Schramm and H. Stoecker, Phys. Rev. C **101**, 034904 (2020).
- [45] P. Bonche and D. Vautheran, Nucl. Phys. A**372**, 496 (1981).
- [46] B. D. Serot and J. D. Walecka, Adv. Nucl. Phys. **16**, 1 (1986); Int. J. Mod. Phys. E **6**, 515 (1997).
- [47] J. D. Walecka, Ann. Phys. **83**, 491 (1974).
- [48] R. Manka and I. Bednarek, J. Phys. G Nucl. Part. Phys. **27**, 1975 (2001).
- [49] B. ter Haar and R. Malfliet, Phys. Rep. **149**, 207 (1987); R. Brockman and R. Malfliet, Phys. Rev. C**42**, 1965 (1990).
- [50] C. Sasaki, K. Morita, P. M. Lo and K. Redlich, Nucl. Phys. A **982**, 219, (2019).
- [51] B. Abelev *et al.* [ALICE Collaboration], Phys. Rev. C **88**, 044910 (2013).
- [52] B. B. Abelev *et al.* [ALICE Collaboration], Phys. Rev. Lett. **111**, 222301 (2013).
- [53] B. B. Abelev *et al.* [ALICE Collaboration], Phys. Lett. B **728**, 216 (2014); **734**, 409 (2014).
- [54] A. Andronic, P. Braun-Munzinger, B. Friman, P. M. Lo, K. Redlich and J. Stachel, Phys. Lett. B **792**, 304 (2019).
- [55] P. M. Lo, Phys. Rev. D **102**, 034038 (2020).
- [56] A. Bazavov *et al.* [HotQCD], Phys. Rev. D **90**, 094503 (2014).
- [57] S. Borsanyi, Z. Fodor, C. Hoelbling, S. D. Katz, S. Krieg and K. K. Szabo, Phys. Lett. B **730**, 99 (2014).
- [58] A. Khuntia, S. K. Tiwari, P. Sharma, R. Sahoo and T. K. Nayak, Phys. Rev. C **100**, 014910 (2019).

- [59] P. Garg, D. K. Mishra, P. K. Netrakanti, B. Mohanty, A. K. Mohanty, B. K. Singh and N. Xu, Phys. Lett. B **726**, 691 (2013).
- [60] M. Mukherjee, S. Basu, A. Chatterjee, S. Chatterjee, S. P. Adhya, S. Thakur and T. K. Nayak, Phys. Lett. B **784**, 1 (2018).